Temperature-Dependent Gelation Behaviour of Double Responsive P2VP-*b*-PEO-*b*-P(GME-*co*-EGE) Triblock Terpolymers: A SANS Study

Matthias Karg,[1] *Stefan Reinicke,*[2] *Alain Lapp,*[3] *Thomas Hellweg,**[4] *Holger Schmalz**[2]

Summary: Aqueous solutions of a double responsive $P2VP_{62}$-*b*-PEO_{452}-*b*-P(GME_{36}-*co*-EGE_{36}) triblock terpolymer were investigated by means of small-angle neutron scattering (SANS) in order to derive information about structural changes going along with the temperature triggered gel-sol-gel transition at pH = 7, and the sol-gel transition at pH = 3.5, respectively, observed by rheology. SANS measurements on dilute samples at different pH and temperature confirmed the formation of core-shell-corona micelles under conditions, where only one of the outer blocks is insoluble. In addition, temperature-dependent scattering experiments were performed for higher volume fractions, that is, the concentration range where hydrogels were formed. This allowed us to identify the structural transitions, being responsible for the gel-sol-gel transition at pH = 7, and the structure of the gel phase formed at low pH and elevated temperatures.

Keywords: block copolymers; neutron scattering; responsive hydrogels; rheology; smart materials

Introduction

''Smart'' hydrogels are water-based polymeric networks, which respond with a significant change of a property on small changes in their physical and/or chemical environment. Suitable stimuli, that can be used to trigger a corresponding property change of the hydrogel, are pH, temperature, ionic strength, or the application of external magnetic and electric fields.[1–5] ''Smart'' hydrogels are commonly classified according to their network type, that is, chemically or physically crosslinked. Chemically crosslinked stimuli-responsive polymers form gels that can swell or shrink upon changes in external parameters like temperature or pH.[6–9] However, the shape and mechanical properties of the chemically crosslinked hydrogels are fixed once the gel is formed. To overcome these limitations, many recent concepts of ''smart'' hydrogels are based on ABA, ABC, $(AB)_x$ and ABCBA block copolymer structures, which are amphiphilic only under certain conditions. Here, an external stimulus triggers the formation or breakup of physical network junctions, which in turn leads to a reversible gel formation/disintegration.[10–18]

''Smart'' hydrogels play an important role in biomedical applications like drug delivery and tissue engineering.[2,5,19–23] They are further used in sensors, storage media, actuating systems, or microfluidic switches.[24–30] With respect to applications, systems responding to more than only one stimulus are of potential interest. However,

[1] Bio21 Institute & School of Chemistry, University of Melbourne, 3010 Victoria, Australia
[2] Makromolekulare Chemie II, Universität Bayreuth, D-95440 Bayreuth, Germany
E-mail: holger.schmalz@uni-bayreuth.de
[3] Laboratoire Léon Brillouin, CEA de Saclay, 99191 Gif sur Yvette, France
[4] Physikalische und Biophysikalische Chemie (PC III), Fakultät für Chemie, Universität Bielefeld, D-33615 Bielefeld, Germany
E-mail: thomas.hellweg@uni-bielefeld.de

the number of physical hydrogels which are multiple stimuli-responsive is still limited. Dual responsive hydrogels, being responsive to pH and temperature, were realized based on poly(N,N–diethylacrylamide)-*block*-poly(acrylic acid)-*block*-poly(N,N-diethylacrylamide) (PDEAAm-*b*-PAA-*b*-PDEAAm) ABA triblock copolymers,[16] ABCBA pentablock terpolymers, where A is a pH-sensitive poly(sulfamethazine methacrylate) block, B is poly(ε-caprolactone) (PCL), and C is poly(ethylene oxide) (PEO),[11] and multiblock or star-shaped copolymers composed of PEO and poly(amino urethane).[31,32] Alternatively, pH- and temperature-responsive hydrogels can be constructed from PEO-*block*-poly(L-glutamic acid) diblock copolymers utilizing host-guest interactions between PEO and α-cyclodextrin.[33] A very recent example is based on hybrid inclusion complexes (HICs) between an azobenzene end-functionalized poly(*N*,*N*-dimethylacrylamide)-*block*-poly(N-isopropylacrylamide) diblock copolymer (AZO-(PDMAAm-*b*-PNIPAAm)) and β-cyclodextrin functionalized quantum dots, resulting in a hydrogel which responds to temperature and various substances, such as 1-adamantylamine, through a supramolecular substitution process.[34]

Recently, we reported on a new approach towards double stimuli-sensitive hydrogels, being responsive to both pH and temperature, based on ABC triblock terpolymers.[35] The triblock terpolymers are composed of a water soluble PEO middle block, a pH-sensitive poly(2-vinylpyridine) (P2VP) A block, and a thermo-sensitive poly(glycidyl methyl ether-*co*-ethyl glycidyl ether) P(GME-*co*-EGE) C block. At pH = 7, where the P2VP block is hydrophobic, and sufficiently high concentration a gel-sol-gel transition was observed upon heating. Small-angle neutron scattering (SANS) experiments on dilute and concentrated samples revealed, that the low temperature gel state at pH = 7 is based on a body centered cubic (bcc) packing of core-shell-corona (CSC) micelles consisting of a P2VP core, a PEO shell, and a thermo-sensitive P(GME-*co*-EGE) corona (Scheme 1).[35,36] At pH = 3.5, the P2VP block is protonated and thus water-soluble. Upon heating, the thermo-sensitive P(GME-*co*-EGE) block becomes insoluble at temperatures above the respective cloud point (T_{CP}) and consequently a temperature-

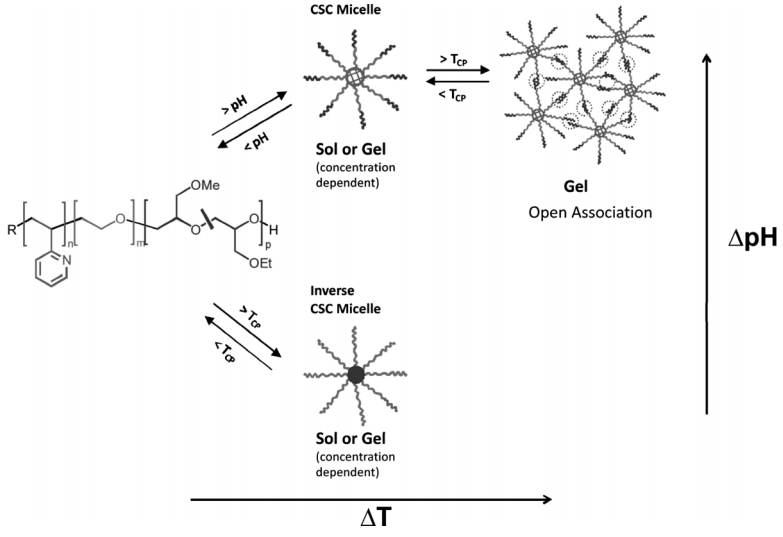

Scheme 1.
Scheme of the formation of double responsive hydrogels based on P2VP-*b*-PEO-*b*-P(GME-*co*-EGE) triblock terpolymers.

induced gelation was observed, presumably due to the formation of a close packing of inverse CSC micelles with a collapsed P(GME-*co*-EGE) core (Scheme 1).

In our previous work, we focused on the structure determination of the low temperature gel phase formed at pH = 7.[35,36] However, the structural changes being responsible for the observed gel-sol-gel transition upon heating at pH = 7 were not addressed. As depicted in Scheme 1, the high temperature gel phase is expected to result from an open association of the CSC micelles, since the thermo-sensitive micellar corona collapses above the cloud point of the P(GME-*co*-EGE) block and forms the network junctions. In addition, the structure of the hydrogel formed by inverse CSC micelles at low pH and elevated temperatures has not been verified yet.

In this paper we present temperature-dependent SANS measurements providing missing information about the mechanism of the gel-sol-gel transition at pH = 7, and the internal structure of the hydrogel formed at low pH and elevated temperatures.

Experimental Part

Materials

The $P2VP_{62}$-*b*-PEO_{452}-*b*-P(GME_{36}-*co*-EGE_{36}) triblock terpolymer was synthesized via sequential anionic polymerization according to the procedure described elsewhere.[35,37] D_2O (99.9%, Deutero GmbH), concentrated DCl (36–38% in D_2O, Deutero GmbH), concentrated HCl (Riedel-de-Haën), and 1 M NaOH (Titrisol, Merck) were used as received. A 1 M NaOD solution was prepared by diluting a NaOD stock solution (40% in D_2O, Deutero GmbH) using D_2O.

Sample Preparation

For SANS investigations the desired amount of the triblock terpolymer was dissolved in pure D_2O, or H_2O/D_2O mixtures for contrast variation experiments. The apparent pH was adjusted to a value of 3–4 using concentrated DCl in order to protonate the P2VP block, rendering it hydrophilic. This ensures molecular dissolution of the polymer. The solution was either kept at the low pH or titrated slowly to $pH_{app} = 7$ (titer 1 M NaOD, dosing rate 1.3 μL min^{-1}), causing the deprotonation of the P2VP block and consequently the formation of CSC micelles with a hydrophobic P2VP core.

Samples for rheological investigations were prepared in a similar manner, using deionized water, concentrated HCl, and NaOH (titer 1 M NaOH, dosing rate 0.13–0.67 μL min^{-1}). The titrations and pH-measurements were performed using a titrator (Titrando 809, Metrohm, Herisau, Switzerland), equipped with a titration unit (Dosino 800, Metrohm, Herisau, Switzerland) and a common glass membrane pH-electrode (microelectrode, Metrohm, Herisau, Switzerland).

Test Tube Inversion

The glass tubes (volume 5 mL) containing the samples were immersed into an oil bath, which was heated stepwise (1 K min^{-1}) using a heating plate (RCT basic, IKA) equipped with a contact thermometer (Ikatron, IKA). After each temperature step the test tubes were inverted in order to check whether the sample flows or not.

Rheology

For dynamic-mechanical measurements a Physica MCR 301 rheometer (Anton Paar GmbH, Germany) with a cone-and-plate shear cell geometry ($D = 50$ mm, cone angle = 1°) was used. Prior to the measurements the linear viscoelastic regime for each sample was determined performing a strain sweep test at a frequency of 1 Hz. For all measurements a frequency of 1 Hz, a strain of 0.7%, and a heating rate of 0.1 K min^{-1} were applied. The temperature was controlled by a Peltier element.

Small-Angle Neutron Scattering (SANS)

SANS measurements were performed on the PAXY instrument of the Laboratoire Léon Brillouin (LLB, CEA de Saclay). The

wavelength of the used neutrons was $\lambda = 6$ Å with a spread of $\Delta\lambda/\lambda = 10\%$. A two-dimensional multi-detector was used to collect the scattered neutrons. In order to cover a sufficient q-range, three sample-to-detector distances were chosen (1.05 m, 3.05 m, and 6.75 m). A thermostat combined with a PT 100 temperature sensor was used to control the sample temperature with an accuracy of ± 0.5 °C. The samples were prepared in pure D_2O or mixtures of H_2O and D_2O to vary the scattering contrast. Afterwards, the samples were filled in 1 mm standard quartz cells (Hellma, Germany) and SANS measurements were performed. The collected data were circularly averaged and corrections for electronic noise, detector efficiency, as well as empty cell and solvent scattering were done. The corrected data were brought to an absolute scale by normalisation using the method developed by Cotton. More detailed information on the data treatment procedure of the LLB can be found elsewhere.[38,39] In order to fit the normalised and merged scattering profiles we used the SASfit program by Kohlbrecher.[40]

The employed fits are based on the form factor of a spherical core-shell particle with a corona of Gaussian polymer coils using:

1. The form factor for a spherical core:

$$K(q,R,\Delta\eta) = \frac{4}{3}\pi R^3 \Delta\eta 3 \times \frac{(\sin(qR) - qR\cos(qR))}{(qR)^3} \quad (1)$$

Here, R is the core radius and $\Delta\eta$ the scattering contrast.

2. The form factor for a spherical shell:

$$I(q,R,\nu,\Delta\eta,\mu) = \left[K(q,R,\Delta\eta) - K(q,\nu R,\Delta\eta(1-\mu))\right]^2 \quad (2)$$

Here, R is the outer radius, the fraction νR accounts for the core radius, $\mu\Delta\eta$ defines the scattering contrast of the core, and $\Delta\eta$ is the scattering contrast of the shell.

3. The form factor for Gaussian polymer coils:

$$I(q) = I_0 2\frac{\exp(-u)+u-1}{u^2}, \quad \text{with } u = q^2 R_g^2 \quad (3)$$

Here, R_g is the radius of gyration of the coiled polymer chains in the corona, and I_0 the forward scattering ($q = 0$).

To account for the structure factor of the micelles at higher volume fractions, ϕ, we used a structure factor for sticky hard spheres, $S(q,R_{HS},\phi,\tau)$, according to:

$$S(q,R_{HS},\phi,\tau) = \frac{1}{1-C(q)} \quad (4)$$

Here, $C(q)$ is defined as:

$$\begin{aligned} C(q) &= 2\frac{\eta\lambda}{\kappa}\sin\kappa - 2\left(\frac{\eta\lambda}{\kappa}\right)^2(1-\cos\kappa) \\ &- \left[\alpha\kappa^3(\sin\kappa - \kappa\cos\kappa)\right. \\ &+ \beta\kappa^2\left(2\kappa\sin\kappa - (\kappa^2-2)\cos\kappa - 2\right) \\ &+ \frac{\eta\alpha}{2}\left((4\kappa^3 - 24\kappa)\sin\kappa\right. \\ &\left.\left. - (\kappa^4 - 12\kappa^2 + 24)\cos\kappa + 24\right)\right] \times \frac{24\eta}{\kappa^6} \end{aligned} \quad (5)$$

with

$$\kappa = 2qR_{HS},\ \eta = \phi\left(\frac{2R_{HS}+\Delta}{2R_{HS}}\right)^3,$$

$$\varepsilon = \tau + \frac{\eta}{1-\eta},\ \gamma = \phi\frac{1+\eta/2}{3(1-\eta)^2},$$

$$\lambda = \frac{6}{\eta}\left(\varepsilon - \sqrt{\varepsilon^2-\gamma}\right),$$

$$\mu = \lambda\eta(1-\eta),$$

$$\beta = -\frac{3\eta(2+\eta)^2 - 2\mu(1+7\eta+\eta^2) + \mu^2(2+\eta)}{2(1-\eta)^4},$$

$$\text{and } \alpha = \frac{(1+2\eta-\mu)^3}{(1-\eta)^4}$$

R_{HS} is the hard sphere radius, ϕ the volume fraction, and τ the so-called stickiness parameter. A structure factor for sticky hard spheres was used to account for the fact, that the P(GME-*co*-EGE) block starts to lose some of its water in the hydration shell at temperatures well below

Table 1.
Scattering length densities (SLDs) of the different blocks in P2VP-*b*-PEO-*b*-P(GME-*co*-EGE) triblock terpolymers in comparison to that of D_2O (H_2O).

Sample	Density	SLD	ΔSLD[a)]
	[g cm^{-3}]	[10^{10} cm^{-2}]	[10^{10} cm^{-2}]
D_2O	1.10	6.36	–
H_2O	1.00	-0.56	−6.92
C_7H_7N (P2VP)[b)]	1.15	1.77[41]	−4.59
C_2H_4O (PEO)[b)]	1.13	0.5[42]	−5.86
$C_9H_{18}O_4$ (P(GME-*co*-EGE))[b)]	1.13[c)]	ca. 0.56[d)]	−5.80

[a)]Scattering contrast with respect to D_2O.[b)]Chemical formula of the repeating units; composition of the P(GME-*co*-EGE) block: 50 mol% GME.[c)]Density of P(GME-*co*-EGE) was assumed to be identical to that of amorphous PEO.[d)]Calculated based on the chemical formula of the repeating unit and the scattering lengths of the respective atoms.

its cloud point.[35,36] Consequently, the P(GME-*co*-EGE) corona of the CSC micelles can be considered slightly sticky at ambient temperature.

All fits were performed starting with a linear baseline to account for incoherent scattering, then the core-shell form factor was added using theoretical values for the core and shell scattering contrast (Table 1) and an overall micelle radius estimated from a Guinier analysis of a dilute micellar solution (1.2 wt%, pH = 7, 20 °C). Then, the SANS profiles were fitted using the core radius, overall micelle radius, core contrast, as well as shell contrast as variable parameters. Afterwards, polydispersity of the overall micelle size was taken into account using a Lorentzian size distribution with the volume fraction as scaling parameter. Finally, the Gaussian coil form factor and the structure factor for sticky hard spheres were added. Here, variable parameters were the radius of gyration, the forward scattering, the volume fraction, and the hard sphere radius.

Results and Discussion

Rheology

Before discussing the results from the SANS experiments, we first address the temperature-dependent phase behaviour of concentrated aqueous $P2VP_{62}$-*b*-PEO_{452}-*b*-$P(GME_{36}$-*co*-$EGE_{36})$ (subscripts denote the average degree of polymerization of the corresponding block) solutions. Figure 1 shows the temperature-dependent storage (G') and loss (G'') modulus for an 18 wt% solution of the triblock terpolymer at two different pH values. Regimes with $G' > G''$ are referred to as gel state with

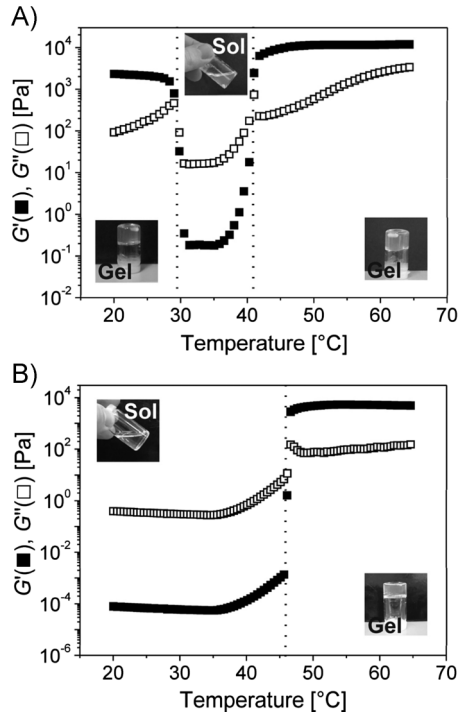

Figure 1.
Temperature dependence of *G*' and *G*'' for an 18 wt% solution of $P2VP_{62}$-*b*-PEO_{452}-*b*-$P(GME_{36}$-*co*-$EGE_{36})$: A) at pH = 7, and B) at pH = 3.5 (0.1 K min^{-1}, $\gamma = 0.7\%$). The photographs show results from the respective test tube inversion experiments.

respect to common definitions.[43] Sol states on the other hand are characterized by a loss modulus being significantly larger compared to the storage modulus, that is, $G'' > G'$. Commonly, a storage modulus in the gel state exceeding the critical value of $G' = 1$ kPa is taken as the criterion for the presence of a strong free-standing gel.[44]

At pH = 7 a gel-sol-gel transition takes place, which is accompanied with a strengthening of the gel (Figure 1A). The high storage moduli of the low ($G'(20\,^{\circ}C) = 2.3$ kPa) and high ($G'(65\,^{\circ}C) = 12$ kPa) temperature gel phases, and the corresponding photographs from test tube inversion experiments reveal the presence of strong free-standing gels at room temperature as well as at elevated temperatures. In our previous work we could identify the low temperature gel phase as a body centered cubic packing of CSC micelles with P2VP cores.[36] The high temperature gel phase, however, is assumed to be formed by an open association of the CSC micelles, as the P(GME-*co*-EGE) corona chains become insoluble at $T > 40\,^{\circ}C$,[35] which leads to a physical crosslinking of the micelles (Scheme 1). The validity of the proposed mechanism for the observed gel-sol-gel transition and the underlying structural changes will be addressed in detail in the following sections dealing with the temperature-dependent SANS results.

Figure 1B depicts the temperature-dependent evolution of the dynamic moduli of the same sample at pH = 3.5. At low pH the P2VP block is protonated and thus water-soluble. As a result, the triblock terpolymer is molecularly dissolved at room temperature and pH = 3.5 and the solution appears as a clear free-flowing liquid of low viscosity. Upon increasing temperature the sol transforms into a free-standing gel ($G'(65\,^{\circ}C) = 4.9$ kPa) at about 46 °C, as indicated by the crossover of the G' and G'' graphs. This is most likely attributed to the formation of a close packing of inverse CSC micelles with P(GME-*co*-EGE) cores (Scheme 1), as the thermo-responsive P(GME-*co*-EGE) block becomes insoluble at $T > 40\,^{\circ}C$.[35] It is noted, that the storage modulus of the gel phase formed at pH = 3.5 and elevated temperatures (Figure 1B) is approximately twice as high compared to that of the gel phase formed at pH = 7 and room temperature (Figure 1A), although both gels presumably consist of a close cubic packing of micelles of comparable dimensions. This might result from the charged P2VP corona of the inverse CSC micelles formed at low pH and high temperature, inducing an increase in the intermicellar repulsion due to electrostatic interactions and thus an increased effective volume fraction of the CSC micelles.

Internal Structure of the Micellar Aggregates

At the beginning, we will discuss the results obtained from SANS measurements on dilute samples at pH = 7 /20 °C and pH = 3/ 60 °C, that is, under conditions where only one of the two outer blocks is insoluble (Scheme 1). Accordingly, we should either deal with core-shell-corona (CSC) micelles with P2VP cores (pH = 7, 20 °C), or with inverse CSC micelles with P(GME-*co*-EGE) cores (pH = 3, 60 °C).

In our previous work, we have used a core-shell model with additional Gaussian coils accounting for the soft corona to fit the SANS trace obtained for a dilute solution of CSC micelles (P2VP core).[35] This basic model had some limitations in describing the scattering profile in the low q-range, where structure factor contributions become relevant. Here, we extend our previous work and analyse the data applying a more sophisticated model, which also accounts for intermicellar interactions even at concentrations as low as 1.2 wt% by including a structure factor contribution. Figure 2A shows the SANS intensity profile for a 1.2 wt% solution of $P2VP_{62}$-*b*-PEO_{452}-*b*-P(GME_{36}-*co*-EGE_{36}) at pH = 7 and 20 °C. It can be clearly seen, that the more complex model used within this work describes the data very well even in the low q-range. The contribution of the structure factor basically shows that the micelles are not fully independent of each other even under the established dilute

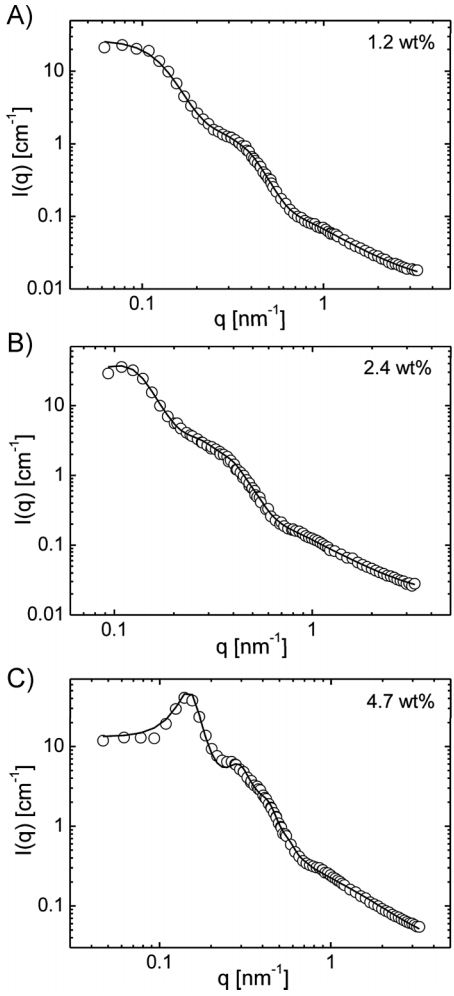

Figure 2.
SANS data for solutions of P2VP$_{62}$-*b*-PEO$_{452}$-*b*-P(GME$_{36}$-*co*-EGE$_{36}$) in D_2O at 20 °C and pH = 7: A) 1.2 wt%, B) 2.4 wt%, and C) 4.7 wt%. The solid lines are fits with a core–shell model plus Gaussian coils, including a structure factor contribution.

conditions. From the shown fit, an overall micelle radius of 18.8 nm as well as a radius of the P2VP core of 5.6 nm could be determined (Table 2). The obtained scattering contrasts for the core and shell (Table 2) show slight deviations compared to the respective theoretical values (Table 1). This can be attributed to a swelling of the shell and the core by D_2O. Thus, from a comparison with the theoretical scattering contrasts D_2O contents of about 90% in the shell and about 20% in the core can be estimated. In addition, the radius of gyration for the Gaussian coils in the corona is found to be 1.6 nm. These results are consistent with the expected formation of CSC micelles with P2VP cores at pH = 7 and room temperature.

The used fitting model has the advantage that it can also be applied to more concentrated solutions of CSC micelles. Figure 2B, 2C give the SANS profiles for a 2.4 wt% and a 4.7 wt% solution of P2VP$_{62}$-*b*-PEO$_{452}$-*b*-P(GME$_{36}$-*co*-EGE$_{36}$), respectively. Especially the SANS profile of the 4.7 wt% solution already shows a pronounced structure factor maximum. The presented fits were constructed using the parameters obtained for the 1.2 wt% solution and allowing only variations in the volume fraction of the micelles and the incoherent background scattering (Table 2). The good agreement between the scattering data and the obtained fits affirms the applicability of the used fitting model.

To further prove whether the P2VP block is the core forming block under these conditions (pH = 7, 20 °C), we performed SANS measurements at various scattering contrasts using mixtures of H_2O and D_2O as solvent. Figure 3A shows the respective SANS profiles for various H_2O/D_2O mixtures. For the data evaluation we used the same model as applied in Figure 2, only allowing variations in the scattering contrasts and the incoherent background scattering (baseline). It can be clearly seen, that the resulting fits describe the scattering profiles very well. From these fits the scattering contrasts of the soluble PEO-*b*-P(GME-*co*-EGE) "shell" ($\Delta\eta$) and the P2VP core ($\mu\Delta\eta$), respectively, were obtained and are plotted as a function of the scattering length density (SLD) of the solvent mixture in Figure 3B. From a linear fit of the data the SLD of the solvent mixture for which zero scattering contrast is reached can be easily extracted. As a result, zero contrast for the PEO-*b*-P(GME-*co*-EGE) "shell" is obtained at a solvent SLD of $0.8 \cdot 10^{10}\,cm^{-2}$, which is close to the

Table 2.
Summary of micelle characteristics obtained from fits of the SANS intensity profiles for solutions of $P2VP_{62}$-*b*-PEO_{452}-*b*-$P(GME_{36}$-*co*-$EGE_{36})$ in D_2O at different pH and temperature.[a)]

	pH = 7			pH = 7	pH = 3
	20 °C			35 °C	60 °C
$c_{Polymer}$ [wt%]	1.2	2.4	4.7	1.2	1.2
core	P2VP	P2VP	P2VP	P2VP	P(GME-*co*-EGE)
R_{core} [nm]	5.6	5.6	5.6	5.6	7.5
$R_{micelle}$ [nm]	18.8	18.8	18.8	17.8	16.7
R_g [nm]	1.6	1.6	1.6	1.4	1.1
$\mu\Delta\eta$ [10^{10} cm^{-2}]	−3.7	−3.7	−3.7	−3.8	−2.2
$\Delta\eta$ [10^{10} cm^{-2}]	−0.23	−0.23	−0.23	−0.28	−0.32
ϕ	0.1	0.2	0.4	0.1	0.1

[a)] R_{core} = radius of the micellar core; $R_{micelle}$ = outer radius of the micelles; R_g = radius of gyration for the Gaussian coils in the micellar corona; $\mu\Delta\eta$ = scattering contrast of the core, and $\Delta\eta$ = scattering contrast of the shell + corona (both with respect to D_2O); ϕ = volume fraction of the micelles.

theoretical SLDs of the respective PEO and P(GME-*co*-EGE) blocks (Table 1). In contrast, zero scattering contrast for the core is reached at $2.1 \cdot 10^{10}$ cm^{-2}, which is in agreement with the expected SLD of the P2VP block. Consequently, the contrast variation experiments clearly confirm that the P2VP block forms the core of the CSC micelles, whereas the PEO middle block and the P(GME-*co*-EGE) outer block form the soluble micellar shell and corona, respectively.

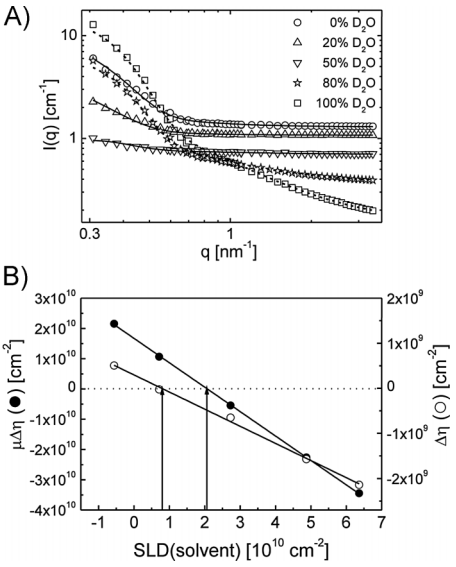

Figure 3.
A) SANS data for solutions of $P2VP_{62}$-*b*-PEO_{452}-*b*-$P(GME_{36}$-*co*-$EGE_{36})$ in different H_2O/D_2O mixtures at 20 °C and pH = 7. The solid lines are fits with a core–shell model plus Gaussian coils, including a structure factor contribution. B) Scattering contrast for the PEO-*b*-P(GME-*co*-EGE) ''shell'' ($\Delta\eta$) and the P2VP core ($\mu\Delta\eta$), obtained from the fits shown in A), as a function of the scattering length density (SLD) of the solvent mixture. The black solid lines are linear fits and the arrows indicate zero contrast.

The established fitting procedure was also applied for the temperature-dependent SANS measurements on 1.2 wt% solutions of $P2VP_{62}$-*b*-PEO_{452}-*b*-$P(GME_{36}$-*co*-$EGE_{36})$ at different pH values. First, we discuss the SANS profile and the corresponding fit results obtained for CSC micelles at pH = 7 and 35 °C (Figure 4A, Table 2). The radius of the P2VP core (R_{core} = 5.6 nm) is identical to the value for the corresponding CSC micelles at 20 °C. This is reasonable, as the P2VP block is completely deprotonated and thus strongly collapsed at pH = 7, that is, the P2VP core of the CSC micelles is ''frozen''. This is supported by ^{1}H-NMR data (results not shown), revealing a disappearance of signals attributable to the 2VP units at pH > 5. In contrast, the overall micelle radius at 35 °C ($R_{micelle}$ = 17.8 nm) is slightly decreased with respect to the value at 20 °C ($R_{micelle}$ = 18.8 nm). Consequently, the radius of the soluble PEO-*b*-P(GME-*co*-EGE) ''shell'' is smaller. In addition, the ''shell'' shrinkage goes along with a slightly increased scattering contrast $\Delta\eta$, which points to a slightly decreased D_2O content in the PEO-*b*-P(GME-*co*-EGE) ''shell'' (Table 2). These

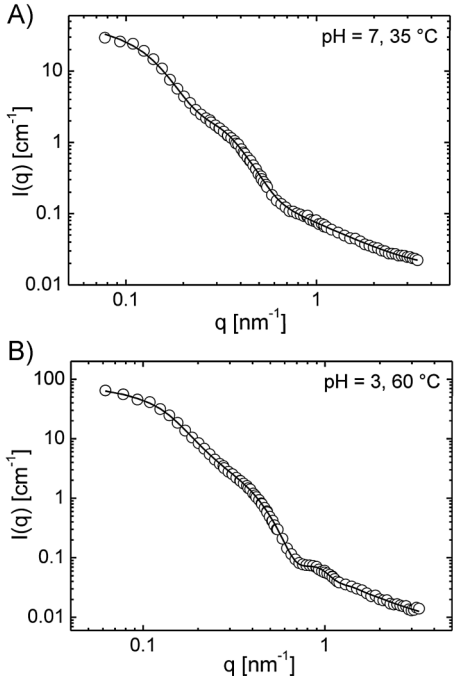

Figure 4.
SANS data for 1.2 wt% solutions of $P2VP_{62}$-*b*-PEO_{452}-*b*-P(GME_{36}-*co*-EGE_{36}) in D_2O: A) 35 °C, pH = 7; and B) 60 °C, pH = 3. The solid lines are fits with a core–shell model plus Gaussian coils, including a structure factor contribution.

results can be attributed to a shrinkage of the P(GME-*co*-EGE) block next to its cloud point (T_{CP} ca. 40 °C[35]), similar to the behaviour of PEO but at significantly lower temperatures.[45–49] The observed shrinkage of the CSC micelles with P2VP cores is important later on in the discussion on the mechanism of the temperature-induced gel-sol-gel transition at pH = 7.

Figure 4B shows the SANS profile and the corresponding fit for the same solution at pH = 3 and T = 60 °C. Under these conditions only the P(GME-*co*-EGE) block is insoluble and the formation of inverse CSC micelles with P(GME-*co*-EGE) cores is expected (Scheme 1). The radius of the P(GME-*co*-EGE) core (R_{core} = 7.5 nm) is about 30% larger compared to the core radius of the CSC micelles with P2VP cores formed at pH = 7 (R_{core} = 5.6 nm). Moreover, the obtained scattering contrast of the core (Table 2) is smaller compared to the expected value (Table 1). These results indicate, that the thermo-sensitive P(GME-*co*-EGE) core is still swollen with D_2O to a certain extent. The overall micelle radius of the inverse CSC micelles ($R_{micelle}$ = 16.7 nm) is reduced with respect to the value of the CSC micelles formed at pH = 7 (Table 2). Consequently, the soluble PEO-*b*-P2VP "shell" of the inverse CSC micelles (d_{shell} ca. 9.2 nm) is significantly smaller compared to the PEO-*b*-P(GME-*co*-EGE) "shell" of the CSC micelles (d_{shell} ca. 12.2 nm at 35 °C and pH = 7). This goes along with a significantly increased scattering contrast of the "shell", and thus can be explained by the commonly observed shrinkage of the PEO block at elevated temperatures.[45–49]

It is finally noted, that the intensity profile obtained at pH = 3 and T = 60 °C exhibits a shoulder in the high q-range, which was fitted assuming the presence of unimolecular micelles, that is, single triblock terpolymer chains with a collapsed P(GME-*co*-EGE) block shielded by the hydrophilic P2VP (protonated at pH = 3) and PEO blocks, along with inverse CSC micelles. Applying this procedure, a radius of gyration for the unimolecular micelles of 6 nm was obtained. Consequently, we might deal with an equilibrium between unimers and chains aggregated into inverse CSC micelles in dilute solutions. Such an equilibrium state seems to be likely since the P(GME-*co*-EGE) block is swollen to a certain extent, and therefore the chains are still expected to be mobile.

Structure of the Hydrogel Formed at Low pH and Elevated Temperatures

Figure 5 shows the SANS intensity profile of a concentrated solution (14.3 wt%) of $P2VP_{62}$-*b*-PEO_{452}-*b*-P(GME_{36}-*co*-EGE_{36}) at pH = 3 and T = 60 °C. Under these conditions, the form factor is overlapped by a pronounced structure factor. Analogous to the gel phase formed at pH = 7 and room temperature,[35] we observe higher order reflections at relative peak positions of $1:2^{1/2}:3^{1/2}$, which points to the presence of

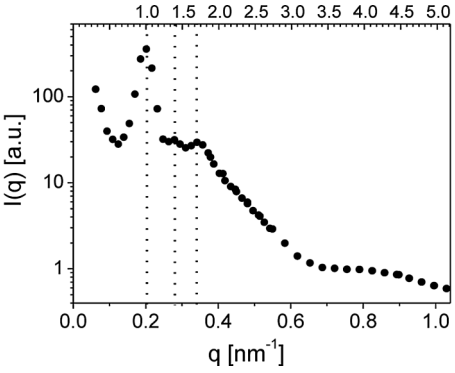

Figure 5.
SANS data for a 14.3 wt% solution of $P2VP_{62}$-*b*-PEO_{452}-*b*-P(GME_{36}-*co*-EGE_{36}) in D_2O at $T = 60\,^{\circ}C$ and pH = 3, top x-axis normalized to 1st order reflection. The dotted lines indicate the position of the peak maxima.

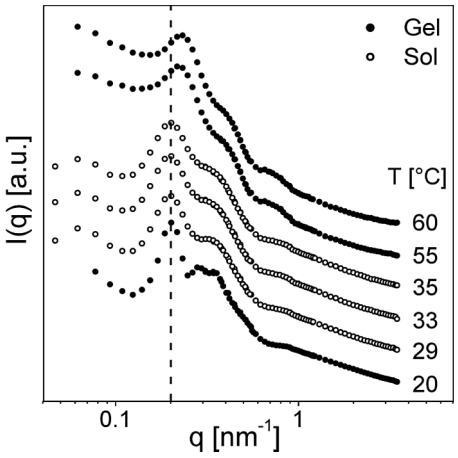

Figure 6.
SANS data for a 14.3 wt% solution of $P2VP_{62}$-*b*-PEO_{452}-*b*-P(GME_{36}-*co*-EGE_{36}) in D_2O at pH = 7 and different temperatures. The curves were shifted vertically for clarity. The dotted line indicates the position of the 1st order reflection for the hydrogel formed at room temperature.

either a simple or a body centered cubic packing of inverse CSC micelles with P(GME-*co*-EGE) cores. Taking into account that micelles acting as ''soft'' spheres, that is, the soluble blocks are significantly larger compared to the core forming block, usually form bcc-type structures,[50–59] we can assume that a bcc packing is formed in our case, too. This is further supported by the fact, that the corresponding hydrogel formed at pH = 7 and room temperature was found to exhibit a twinned bcc structure.[36]

Mechanism of the Temperature-Induced Gel-Sol-Gel Transition at pH = 7

In the last part, we want to address the temperature-induced structural changes in a concentrated solution of $P2VP_{62}$-*b*-PEO_{452}-*b*-P(GME_{36}-*co*-EGE_{36}) at pH = 7 that induce the observed gel-sol-gel transition (Figure 1A). Figure 6 shows the SANS intensity profiles for a 14.3 wt% solution of the triblock terpolymer at pH = 7 and different temperatures. Three different structural states can be clearly detected in dependence on temperature, which correlate well with the gel-sol-gel transition observed by rheology. At temperatures below 29 °C a pronounced structure factor with higher order reflections at the relative peak positions of $1:2^{1/2}:3^{1/2}$ indicates the presence of a close cubic packing of CSC micelles with P2VP cores, which is consistent with the observed low temperature gel phase in rheology (Figure 1A). As already pointed out above, this gel phase exhibits a twinned bcc structure.[36] Upon a further increase in temperature, however, the higher order reflections disappear. This points to a disintegration of the cubic lattice, and consequently the gel transforms into a sol. The disintegration of the close packed cubic structure originates from a shrinkage of the CSC micelles, as shown by the corresponding fit of the SANS profile for the 1.2 wt% solution at pH = 7 and $T = 35\,^{\circ}C$ (Table 2, Figure 4A). At even higher temperatures ($T > 40\,^{\circ}C$) we observe a significant shift of the structure factor maximum, q_{max}, to higher values, that is, the average distance between the CSC micelles decreases. This in turn is consistent with the proposed open association of CSC micelles at temperatures above the cloud point of the P(GME-*co*-EGE) block, resulting in a physical crosslinking of the CSC micelles via the now insoluble corona (Scheme 1). In contrast to the low temperature gel phase, this phase does not exhibit long-range order and only shows a glass-like correlation

peak. Accordingly, the proposed mechanism for the observed gel-sol-gel transition is confirmed by the temperature-dependent SANS data.

Conclusion

Concentrated solutions of a double responsive $P2VP_{62}$-*b*-PEO_{452}-*b*-P(GME_{36}-*co*-EGE_{36}) triblock terpolymer form hydrogels under conditions where only one of the end blocks is insoluble. Furthermore, at pH = 7 a temperature-induced gel-sol-gel transition was observed. SANS measurements on aqueous solutions of $P2VP_{62}$-*b*-PEO_{452}-*b*-P(GME_{36}-*co*-EGE_{36}) at different concentrations, pH, and temperature were performed in order to investigate the internal structure of the micellar aggregates and the corresponding hydrogels formed at sufficiently high concentrations, as well as the structural changes being responsible for the observed gel-sol-gel transition.

The SANS intensity profiles of dilute solutions at different pH/temperature were fitted with a core-shell model including a structure factor contribution in order to account for intermicellar interactions in the investigated concentration range. The analysis confirmed the presence of core-shell-corona (CSC) micelles under conditions where only one of the outer blocks is insoluble, that is, CSC micelles with P2VP cores at pH = 7/room temperature, and inverse CSC micelles with P(GME-*co*-EGE) cores at pH = 3/elevated temperatures. The inverse CSC micelles (P(GME-*co*-EGE) core) exhibited an increased core radius compared to that of the CSC micelles (P2VP core), which was attributed to a higher degree of swelling of the P(GME-*co*-EGE) core. The overall size of the CSC micelles, on the other hand, showed a slight decrease upon increasing the temperature to 35 °C, which goes along with a reduced solvent content in the shell. This results from the shrinkage of the P(GME-*co*-EGE) block next to its cloud point (T_{CP} ca. 40 °C) and a partial dehydration of the shell forming PEO block.

In analogy to the gel phase formed at pH = 7 and room temperature (bcc packing of CSC micelles), the scattering profile of the gel phase formed at pH = 3 and $T = 60$ °C showed a pronounced structure factor contribution with higher order reflections at relative peak positions of $1:2^{1/2}:3^{1/2}$, too. Consequently, the hydrogel formed at pH = 3 and elevated temperatures could be assigned to a close cubic packing of inverse CSC micelles with P(GME-*co*-EGE) cores.

Furthermore, the proposed mechanism for the temperature-induced gel-sol-gel transition at pH = 7 could be verified from the scattering experiments. First, the gel phase formed at pH = 7 and room temperature transforms into a sol due to a disintegration of the close cubic packing of CSC micelles, manifested by the disappearance of higher order reflections. This was attributed to the temperature-induced shrinkage of the CSC micelles. Upon a further increase in temperature above the cloud point of the P(GME-*co*-EGE) corona blocks, a significant shift of q_{max} to higher values was observed. This points to a decreasing intermicellar distance, which is consistent with a physical crosslinking of the CSC micelles by the now insoluble corona blocks, that is, an open association of the CSC micelles.

Acknowledgements: The authors acknowledge the German Science Foundation (priority program SPP 1259) for financial support. M.K. is grateful to the Alexander von Humboldt foundation for a Feodor-Lynen research fellowship.

[1] "*Responsive Gels: Volume Transitions I/II*", in: Adv. Polym. Sci., K. Dušek, Ed., Springer, Berlin 1993.
[2] S-k. Ahn, R. M. Kasi, S.-C. Kim, N. Sharma, Y. Zhou, *Soft Matter* **2008**, *4*, 1151.
[3] E. S. Gil, S. M. Hudson, *Prog. Polym. Sci.* **2004**, *29*, 1173.
[4] C. Tsitsilianis, *Soft Matter* **2010**, *6*, 2372.
[5] C. He, S. W. Kim, D. S. Lee, *J. Controlled Release* **2008**, *127*, 189.
[6] M. Achilleos, T. Krasia-Christoforou, C. S. Patrickios, *Macromolecules* **2007**, *40*, 5575.

[7] N. A. Hadjiantoniou, C. S. Patrickios, *Polymer* **2007**, *48*, 7041.
[8] S. Nikoletta, K. Ilias, A. Sotirios, T. Constantinos, *Macromol. Rapid Commun.* **2008**, *29*, 130.
[9] F.-J. Xu, E.-T. Kang, K.-G. Neoh, *Biomaterials* **2006**, *27*, 2787.
[10] S. J. Bae, M. K. Joo, Y. Jeong, S. W. Kim, W.-K. Lee, Y. S. Sohn, B. Jeong, *Macromolecules* **2006**, *39*, 4873.
[11] K. Dayananda, B. S. Pi, B. S. Kim, T. G. Park, D. S. Lee, *Polymer* **2007**, *48*, 758.
[12] N. Fechler, N. Badi, K. Schade, S. Pfeifer, J.-F. Lutz, *Macromolecules* **2008**, *42*, 33.
[13] P. D. Iddon, S. P. Armes, *Eur. Polym. J.* **2007**, *43*, 1234.
[14] H.-H. Lin, Y.-L. Cheng, *Macromolecules* **2001**, *34*, 3710.
[15] S. Shinji, K. Shokyoku, A. Sadahito, *J. Polym. Sci., Part A: Polym. Chem.* **2004**, *42*, 2601.
[16] A. A. Sotirios, T. Constantinos, *Macromol. Chem. Phys.* **2006**, *207*, 2188.
[17] J. Adelsberger, A. Kulkarni, A. Jain, W. Wang, A. M. Bivigou-Koumba, P. Busch, V. Pipich, O. Holderer, T. Hellweg, A. Laschewsky, P. Müller-Buschbaum, C. M. Papadakis, *Macromolecules* **2010**, *43*, 2490.
[18] A. P. Vogt, B. S. Sumerlin, *Soft Matter* **2009**, *5*, 2347.
[19] D. S. Hart, S. H. Gehrke, *J. Pharm. Sci.* **2007**, *96*, 484.
[20] L. Klouda, A. G. Mikos, *J. Pharmaceut. Biopharmaceut.* **2008**, *68*, 34.
[21] Y. Tachibana, M. Kurisawa, H. Uyama, T. Kakuchi, S. Kobayashi, *Chem. Lett.* **2003**, *32*, 374.
[22] L. Yu, J. Ding, *Chem. Soc. Rev.* **2008**, *37*, 1473.
[23] A. Hawkins, N. Satarkar, J. Hilt, *Pharm. Res.* **2009**, *26*, 667.
[24] D. J. Beebe, J. S. Moore, J. M. Bauer, Q. Yu, R. H. Liu, C. Devadoss, B.-H. Jo, *Nature* **2000**, *404*, 588.
[25] P. Calvert, P. Patra, D. Duggal, *Proc. SPIE-Int. Soc. Opt. Eng.* **2007**, *6524*, 65240M.
[26] S. Dai, P. Ravi, K. C. Tam, *Soft Matter* **2008**, *4*, 435.
[27] M. Guenther, D. Kuckling, C. Corten, G. Gerlach, J. Sorber, G. Suchaneck, K. F. Arndt, *Sens. Actuators B* **2007**, *126*, 97.
[28] K. Jindrich, *J. Polym. Sci., Part A: Polym. Chem.* **2009**, *47*, 5929.
[29] H. J. van der Linden, S. Herber, W. Olthuis, P. Bergveld, *Analyst* **2003**, *128*, 325.
[30] L. Dong, H. Jiang, *Soft Matter* **2007**, *3*, 1223.
[31] K. Dayananda, C. He, D. K. Park, T. G. Park, D. S. Lee, *Polymer* **2008**, *49*, 4968.
[32] C. T. Huynh, M. K. Nguyen, D. P. Huynh, S. W. Kim, D. S. Lee, *Polymer* **2010**, *51*, 3842.
[33] Y. Chen, X.-H. Pang, C.-M. Dong, *Adv. Funct. Mater.* **2010**, *20*, 579.
[34] J. Liu, G. Chen, M. Guo, M. Jiang, *Macromolecules* **2010**, *43*, 8086.
[35] S. Reinicke, J. Schmelz, A. Lapp, M. Karg, T. Hellweg, H. Schmalz, *Soft Matter* **2009**, *5*, 2648.
[36] S. Reinicke, M. Karg, A. Lapp, L. Heymann, T. Hellweg, H. Schmalz, *Macromolecules* **2010**, *43*, 10045.
[37] A. Ah Toy, S. Reinicke, A. H. E. Müller, H. Schmalz, *Macromolecules* **2007**, *40*, 5241.
[38] A. Brulet, D. Lairez, A. Lapp, J.-P. Cotton, *J. Appl. Crystallogr.* **2007**, *40*, 165.
[39] J. P. Cotton, ''Initial data treatment'', in: *Neutron X-Ray and Light Scattering*, P., Lindner T. Zemb, Eds., Elsevier Science Publishers B.V., **1991**.
[40] J. Kohlbrecher, ''SASfit: A Program for Fitting Simple Structural Models to Small Angle Scattering Data'', Paul Scherrer Institut, Laboratory for Neutron Scattering, CH-5232, Villigen Switzerland, 2008.
[41] Y. I. Yun, R. M. Briber, R. A. Kee, M. Gauthier, *Polymer* **2003**, *44*, 6579.
[42] B. J. Clifton, T. Cosgrove, R. M. Richardson, A. Zarbakhsh, J. R. P. Webster, *Physica B* **1998**, *248*, 289.
[43] H. H. Winter, M. Mours, *Adv. Polym. Sci.* **1997**, *134*, 165.
[44] K. Nishinari, *Prog. Colloid. Polym. Sci.* **2009**, *136*, 87.
[45] V. Castelletto, I. W. Hamley, R. J. English, W. Mingvanish, *Langmuir* **2003**, *19*, 3229.
[46] H. Li, G.-E. Yu, C. Price, C. Booth, E. Hecht, H. Hoffmann, *Macromolecules* **1997**, *30*, 1347.
[47] M. Ogura, H. Tokuda, S.-I. Imabayashi, M. Watanabe, *Langmuir* **2007**, *23*, 9429.
[48] R. K. Prud'homme, G. Wu, D. K. Schneider, *Langmuir* **1996**, *12*, 4651.
[49] M. Vamvakaki, L. Papoutsakis, V. Katsamanis, T. Afchoudia, P. G. Fragouli, H. Iatrou, N. Hadjichristidis, S. P. Armes, S. Sidorov, D. Zhirov, V. Zhirov, M. Kostylev, L. M. Bronstein, S. H. Anastasiadis, *Faraday Discuss.* **2005**, *128*, 129.
[50] E. Eiser, F. Molino, G. Porte, O. Diat, *Phys. Rev. E* **2000**, *61*, 6759.
[51] E. Eiser, F. Molino, G. Porte, X. Pithon, *Rheol. Acta* **2000**, *39*, 201.
[52] A. P. Gast, *Langmuir* **1996**, *12*, 4060.
[53] I. W. Hamley, C. Daniel, W. Mingvanish, S.-M. Mai, C. Booth, L. Messe, A. J. Ryan, *Langmuir* **2000**, *16*, 2508.
[54] G. A. McConnell, A. P. Gast, J. S. Huang, S. D. Smith, *Phys. Rev. Lett.* **1993**, *71*, 2102.
[55] T. Nicolai, L. Benyahia, *Macromolecules* **2005**, *38*, 9794.
[56] M. J. Park, K. Char, J. Bang, T. P. Lodge, *Macromolecules* **2005**, *38*, 2449.
[57] C. Perreur, J.-P. Habas, J. François, J. Peyrelasse, A. Lapp, *Phys. Rev. E* **2002**, *65*, 041802.
[58] J. M. Sebastian, C. Lai, W. W. Graessley, R. A. Register, *Macromolecules* **2002**, *35*, 2707.
[59] H. Tan, H. Watanabe, Polym. J. **2004**, **36,** 430.

